



Curvature fluctuations of fluid vesicles reveal hydrodynamic dissipation within the bilayer

Hammad A. Faizi^a , Rony Granek^b , and Petia M. Vlahovska^{c,d,1}

Affiliations are included on p. 6.

Edited by David Weitz, Harvard University, Cambridge, MA; received July 8, 2024; accepted September 24, 2024

The biological function of membranes is closely related to their softness, which is often studied through the membranes' thermally driven fluctuations. Typically, the analysis assumes that the relaxation rate of a pure bending deformation is determined by the competition between membrane bending rigidity and viscous dissipation in the surrounding medium. Here, we reexamine this assumption and demonstrate that viscous flows within the membrane dominate the dynamics of bending fluctuations of nonplanar membranes with a radius of curvature smaller than the Saffman–Delbrück length. Using flickering spectroscopy of giant vesicles made of dipalmitoylphosphatidylcholine, DPPC:cholesterol mixtures and pure diblock-copolymer membranes, we experimentally detect the signature of membrane dissipation in curvature fluctuations. We show that membrane viscosity can be reliably obtained from the short time behavior of the shape time correlations. The results indicate that the DPPC:cholesterol membranes behave as a Newtonian fluid, while the polymer membranes exhibit more complex rheology. Our study provides physical insights into the time scales of curvature remodeling of biological and synthetic membranes.

lipid bilayer | membrane viscosity | vesicle | curvature fluctuations | polymersome

Bilayers assembled from lipids are the main structural component of the membranes that envelop and compartmentalize biological and synthetic cells (1–3). In living cells, membranes are dynamic structures that undergo continual morphological transformations involving dramatic changes in curvature, such as budding, fission, and fusion (4–8). Lipid bilayers are easily bent by thermal and active forces, and the resulting fluctuations are both biologically relevant [e.g., in membrane remodeling (9), adhesion (10, 11), and nuclear shape dynamics (12, 13)], and of fundamental interest in soft matter physics (14–17). The canonical problem of thermally driven curvature fluctuations of a membrane was first addressed by Brochard and Lennon nearly 50 y ago (18). In this now-standard model, an undulation with wavenumber q of an initially planar membrane—modeled as an incompressible interface with bending rigidity κ —is dissipated only by the viscosity of the surrounding fluid η and relaxes exponentially at a rate $\kappa q^3 / 4\eta$. Notably, membrane viscosity does not affect the dynamics of the curvature fluctuations.

Departure from planar geometry dramatically changes the membrane dynamics (19–27), as in-plane (shear) and out-of-plane (bending) displacements become coupled (20). For a quasi-spherical vesicle, whose shape is described in terms of fluctuating spherical harmonic modes $r_s(\phi, \theta, t) = R(1 + f(\phi, \theta, t))$, $f = \sum f_{\ell m}(t) Y_{\ell m}(\phi, \theta)$, the relaxation rate of a mode amplitude $f_{\ell m}$ is predicted to be (19, 20, 26, 28)

$$\omega(\ell, \kappa, \chi_s) = \frac{\kappa}{\eta R^3} \frac{(\ell - 1)\ell(\ell + 1)(\ell + 2)(\ell(\ell + 1) + \bar{\sigma})}{4\ell^3 + 6\ell^2 - 1 + (4\ell^2 + 4\ell - 8)} \chi_s, \quad [1]$$

where $\chi_s = \eta_m/R\eta$ is a dimensionless membrane viscosity parameter, the ratio of the Saffman–Delbrück length (η_m/η) to the vesicle radius R , and $\bar{\sigma} = \sigma R^2/\kappa$ is the reduced membrane tension. Setting $\chi_s = 0$ reduces Eq. 1 to the result for a nonviscous area-incompressible interface (29) (an area-compressible membrane has been considered in ref. 30). The Brochard–Lennon's result, $\omega(\ell) \simeq \frac{\kappa}{4\eta R^3} \ell^3$, is only valid at short-wavelengths, $\ell \gg \chi_s$. For $\chi_s \gg 1$, another regime is predicted to emerge in the relaxation spectrum for long-wavelength undulations $1 \ll \ell \ll \chi_s$, in which the dissipation is dominated by membrane viscosity, $\omega(\ell) \simeq \frac{\kappa}{4\chi_s \eta R^3} \ell^4$. This suggests that membrane viscosity can be deduced from the relaxation rates of the curvature fluctuations at equilibrium. Since thermal equilibrium is maintained during the experiment, the thermal undulation

Significance

Membranes, primarily composed of lipid bilayers, shape and compartmentalize cells. Cell architecture is highly dynamic, with membrane conformation changing significantly during processes like movement, division, and vesicle trafficking. Fluidity is essential for membrane structural malleability and diverse shapes; however, its role in membrane deformation dynamics is less recognized. Membrane bending, driven by thermal or active forces, is commonly assumed to be damped by viscous losses in the surrounding medium. Here, by examining the equilibrium shape fluctuations of vesicles, we show that dissipation within the membrane controls the undulation dynamics of highly curved membranes. These findings emphasize the crucial role of membrane viscosity in remodeling cellular structures.

Author contributions: All authors designed research, analyzed the data, and wrote the paper; H.A.F. performed the experiments; and R. G. and P. M. V. developed the theory.

The authors declare no competing interest.

This article is a PNAS Direct Submission.

Copyright © 2024 the Author(s). Published by PNAS. This article is distributed under [Creative Commons Attribution-NonCommercial-NoDerivatives License 4.0 \(CC BY-NC-ND\)](#).

¹To whom correspondence may be addressed. Email: petia.vlahovska@northwestern.edu.

This article contains supporting information online at <https://www.pnas.org/lookup/suppl/doi:10.1073/pnas.241355721/DCSupplemental>.

Published October 23, 2024.

dynamics always remain within the linear response regime, unlike some existing methods that rely on large externally imposed perturbations (31–33).

In this work, we report experimental evidence of membrane viscous dissipation in the flickering of giant vesicles. We theoretically analyze the shape fluctuations of a quasi-spherical vesicle and derive the experimental observables sensitive to dissipation: the transverse mean square displacement of a membrane segment and the time autocorrelation function of the Fourier modes representing the contour of the equatorial cross-section. We find that the latter decays at short times as a stretched exponential, with a universal stretching exponent 3/4, when membrane viscosity dominates dissipation, and approaches single exponential relaxation at long times. Since the static mode spectrum is independent of dissipation, we can independently measure both bending rigidity and membrane viscosity by combining static and dynamic fluctuation spectra. We apply this approach to characterize the viscous dissipation in bilayers made of poly(butadiene)-*b*-poly(ethylene oxide) diblock copolymers or lipid bilayers in the liquid ordered state (mixtures of dipalmitoylphosphatidylcholine (DPPC) and cholesterol (Chol)), for which very limited data exists.

Results and Discussion

Autocorrelation Function of the Thermally Excited Membrane Undulations.

In flickering experiments (35, 36), a time series of the equatorial cross-section of a giant quasi-spherical vesicle (radius $R \sim 10 \mu\text{m}$) is recorded. The quasi-circular contour is decomposed in Fourier modes, $r_s(\phi, \pi/2, t) = R \sum u_\nu e^{-i\nu\phi}$. Their autocorrelation function (ACF) picks up all the $m = \nu$ terms of the expansion of the vesicle shape in spherical harmonics (SI Appendix), leading to an ACF in the form

$$\begin{aligned} \text{ACF}(t) &= \langle u_\nu(0) u_\nu^*(t) \rangle \\ &= \sum_{\ell=|\nu|}^{\ell_{\max}} \frac{k_B T}{((\ell-1)(\ell+2)(\ell(\ell+1)\kappa+\delta))} n_{\ell\nu}^2 |P_{\ell\nu}(0)|^2 e^{-\omega(\ell)t}, \end{aligned} \quad [2]$$

where $k_B T$ is the thermal energy (k_B is the Boltzmann constant and T is the temperature), $P_{\ell\nu}$ is the associate Legendre polynomial, and $n_{\ell\nu}$ is a normalization factor (see for definitions SI Appendix).

The mean square amplitude (static spectrum) of the fluctuations, $\langle |u_\nu|^2 \rangle$, obtained from Eq. 2 by setting $t = 0$, depends only on the membrane elastic properties (bending rigidity and tension). Indeed, the fluctuations spectrum shown in Fig. 1B follows bending-dominated scaling (35, 37) (SI Appendix), $\sim 1/\nu^3$. Rescaling the spectrum by the bending rigidity collapses the data (Fig. 1C) and confirms that the static spectrum is controlled solely by bending rigidity.

The decay of the ACF depends on the membrane viscosity and thus can serve as a reporter for dissipation due to in-plane shear flows in the membrane if χ_s is large enough. Dioleoylphosphatidylcholine (DOPC) and stearoyloleoylphosphatidylcholine (SOPC) viscosities are reported to be 4.1 ± 2.6 nPa.s.m and 9.7 ± 5.8 nPa.s.m, respectively (31), corresponding to dimensionless surface viscosities $\chi_s \lesssim 1$ for a typical $10 \mu\text{m}$ Giant unilamellar vesicle (GUV), too small to have a detectable effect on vesicle shape fluctuations; see Fig. 1D. To achieve a lipid bilayer with high viscosity, we choose i) DPPC:Chol mixtures, because they are in the liquid-ordered phase and thus expected to be very viscous (31, 38), and ii) di-block copolymers composed of hydrophilic and hydrophobic blocks, which are known to be very viscous (39). Membrane viscosity measured with the electrodeformation method (31, SI Appendix) yielded 57.6 ± 12.6 nPa.s.m for DPPC:Chol (1:1), 83.6 ± 14.3 nPa.s.m

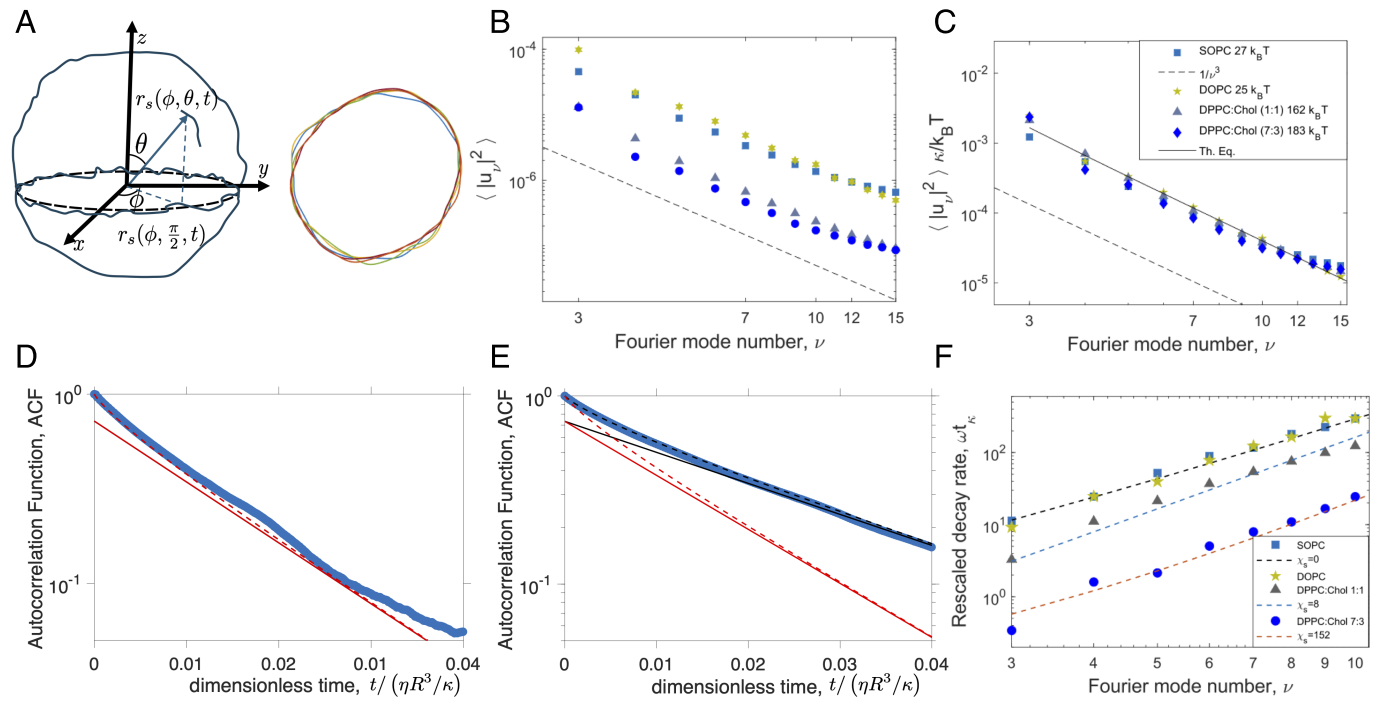


Fig. 1. (A) Sketch of a quasi-spherical vesicle and of time-lapse vesicle contours in the equatorial plane. (B) Power spectrum of the contour fluctuations yields the bending rigidity κ . (C) The rescaled static power spectrum by κ is a universal function of the wavenumber. The solid line is Eq. 2 with $t = 0$. (D and E) Autocorrelation functions (ACF) for Fourier mode 6 of the fluctuating equatorial contours of vesicles made of SOPC (D) and DPPC:Chol (1:1) (E). Blue symbols are the experimental data. Dashed lines are the full theory Eq. 2 and the solid lines are the single exponential decay with rate given by Eq. 1. Red and black line colors correspond to dimensionless membrane viscosity $\chi_s = 0$ and $\chi_s = 8$, respectively. The time scale $t_\kappa = \eta R^3 / \kappa$ is 23.3 s in (D) and 7.6 s in (E). (F) The long-time single exponential decay rate, rescaled by the bending relaxation time, obtained from the ACF as a function of the mode number. The dashed line is the theory Eq. 1.

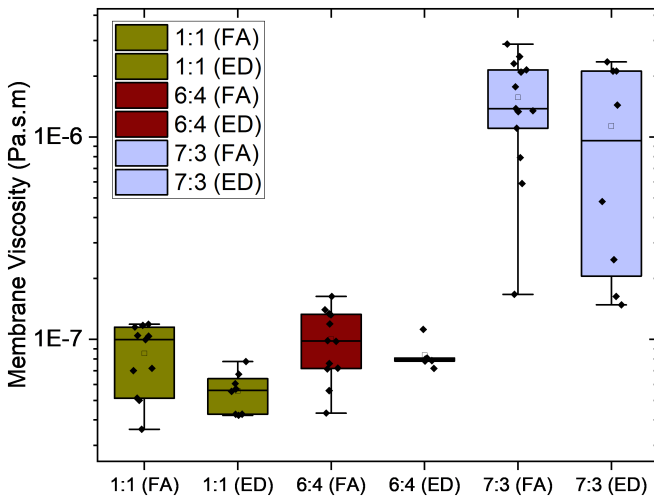


Fig. 2. Membrane viscosity obtained from flickering spectroscopy (FA) and electrodeformation (ED) for different DPPC:Chol mixed bilayers.

for DPPC:Chol (6:4), $1,450 \pm 928$ nPa.s.m for DPPC:Chol (7:3), 14.4 ± 4.4 nPa.s.m for PS0 and 686 ± 51 nPa.s.m for PS1, spanning a range of dimensionless viscosities, ~ 1 to 150. Fig. 1*E* demonstrates that indeed the curvature fluctuations of the DPPC:Chol mixtures relax much more slowly compared to SOPC, indicating significant membrane viscosity, in this case by a factor of 10 larger than the SOPC viscosity.

Obtaining the bending rigidity and tension from the static spectrum leaves only one unknown parameter, the membrane viscosity, in the ACFs of the Fourier modes. The long-time exponential decay can be easily fitted; see solid lines in Fig. 1*D* and *E*. Using this value of the membrane viscosity in Eq. 2 describes well the full relaxation curve (dashed lines). Fig. 1*F* summarizes the relaxation rates obtained from the long-time single exponential fit of mode numbers 3 to 10. The slowing down of the ACF decay suggests that DOPC:Chol mixtures are much more viscous than the bilayers in the liquid disordered phase, DOPC, and SOPC. The dependence of the relaxation rates on mode number is well described by Eq. 1 and yields the membrane viscosity.

The viscosity obtained from the ACF fits agrees well with the data obtained from electrodeformation; see Fig. 2. Membrane viscosity increases sharply with the DPPC fraction, demonstrating that the mixed membrane viscosity is not an additive property of the single-component bilayer properties, as also reported for other mixed systems (40).

Subdiffusive Fluctuation Dynamics. The ACF of the equatorial Fourier mode of order v , Eq. 2, is not a single exponential, unless at sufficiently long times $\omega(v)t \gtrsim 1$, where $\text{ACF} \sim e^{-\omega(v)t}$. At short times, $\omega(v)t \ll 1$, all modes with $\ell \geq |v|$ contribute and the ACF decay is nonexponential, effectively approaching a stretched exponential decay $\sim \exp[-(\gamma(v)t)^\zeta]$ with stretching exponent ζ and relaxation rate $\gamma(v)$. More precisely (see *SI Appendix* for details), there are two “short time” regimes (i.e. for $t \ll \omega(v)^{-1}$), commencing by a regime where dissipation is dominated by the solvent viscosity followed by a membrane viscosity dominated regime. The crossover time separating the two regimes is

$$t^* \approx \frac{4\eta R^3}{\kappa \chi_s^3}. \quad [3]$$

For early times, $t_0 \ll t \ll t^*$, where t_0 is the shortest relaxation time, $t_0 = 1/\omega(\ell_{\max}) \sim \eta d^3/\kappa$, where d is the bilayer thickness, we get for the ACF in the solvent dissipation regime

$$\langle u_v(0)u_v^*(t) \rangle \simeq \langle |u_v|^2 \rangle - \frac{1}{8\pi^2} \frac{k_B T}{\eta R^3} t \left[\frac{1}{3} \ln \left(\frac{4\eta R^3}{\kappa v^3 t} \right) + 0.2838 \right] \quad [4]$$

For later times, $t^* \ll t \ll \omega(v)^{-1}$ —given that such a regime can be manifested, i.e. for $\chi_s \gg v$ —we obtain that the ACF in the membrane dissipation regime is approximated by

$$\langle u_v(0)u_v^*(t) \rangle \simeq \langle |u_v|^2 \rangle - \frac{\Gamma[1/4]}{6\pi^2} \frac{k_B T}{\kappa} \left(\frac{\kappa}{4\chi_s \eta R^3} t \right)^{3/4}, \quad [5]$$

presenting a nonexponential relaxation of the ACF from its static value; it may be cast as

$$\langle u_v(0)u_v^*(t) \rangle \simeq \langle |u_v|^2 \rangle \left(1 - (\gamma(v)t)^\zeta \right), \quad [6]$$

where $\zeta = 3/4$ and the effective relaxation rate $\gamma(v)$ is

$$\gamma(v) = \frac{\Gamma[1/4]^{4/3}}{4} \frac{\kappa v^4}{\chi_s \eta R^3} = \frac{\Gamma[1/4]^{4/3}}{4} \frac{\kappa v^4}{\eta_m R^2}, \quad [7]$$

such that $\gamma(v) = \Gamma[1/4]^{4/3} \omega(v) \sim v^4$.

The mean square displacement of a Fourier mode v is directly related to the ACF, $2\langle |u_v|^2 \rangle - \langle u_v(0)u_v^*(t) \rangle$ (see *SI Appendix* for the derivation). Thus the “stretching” exponent, $\zeta = 3/4$, is equivalent to the anomalous diffusion exponent of equatorial Fourier modes. It is identical to the one governing rod-like semiflexible polymers obeying the worm-like chain model. This is interesting and can be rationalized by the following argument. First, by looking at the Fourier modes of deformations at the equator, the effective dimensionality of the Helfrich bending energy phase space is reduced from two to one, as for semiflexible polymers (41, 42). Second, the membrane viscosity-dominated dissipation suppresses the long-range solvent hydrodynamic interaction, which again leads to a similar behavior as in rod-like semiflexible polymers where the effect of the solvent-mediated hydrodynamic interaction is marginal (logarithmic).

To summarize, if membrane viscosity is dominating the relaxation and mode number is high (such that $\chi_s \gg v \gg 1$), we find that the ACF relaxation profile can be approximated by the following form

$$\langle u_v(0)u_v^*(t) \rangle = \langle |u_v|^2 \rangle U_v[\gamma(v)t], \quad [8]$$

where the scaling function $U_v(y)$ (for $v \gg 1$) obeys

$$U_v(y) \simeq \begin{cases} 1 - y^{3/4} & \text{for } y \ll 1 \\ C_v \exp[-y/\Gamma[1/4]^{4/3}] & \text{for } y \gg 1 \end{cases}, \quad [9]$$

(where C_v is a slowly decreasing function of v .)

Fig. 3 compares the experimental ACFs for dipalmitoylphosphatidylcholine (DPPC):Chol and PS1 systems and the theoretical predictions. The DPPC:Chol (1:1) is only moderately viscous and the long-time single-exponential fit of the ACFs in Fig. 3*A* yield dimensionless viscosity $\chi_s = 5$, corresponding to membrane viscosity 85 nPa.s.m. Accordingly, the short time relaxation of the ACF (and the mean square displacement, MSD), at times shorter than the crossover time t^* , is dominated by the dissipation in the solvent. The DPPC:Chol (7:3) and the

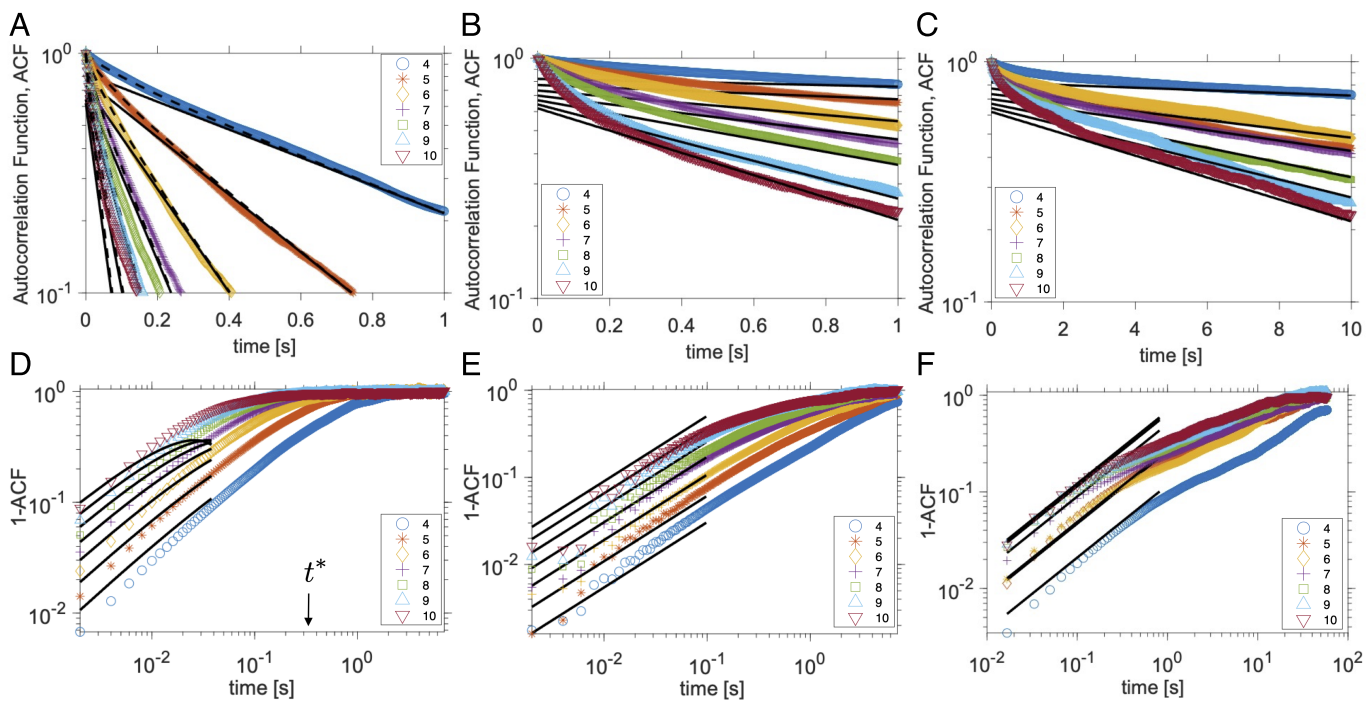


Fig. 3. Normalized autocorrelation functions (ACF) for Fourier modes 4 to 10 of the fluctuating equatorial contour of vesicles made of (A) DPPC:Chol (1:1), (B) DPPC:Chol (7:3), and (C) PS1. Symbols are the experimental data. In (A–C) the dashed lines are the full theory Eq. 2 and the solid lines are the single exponential decay with rate given by Eq. 1. (D–F) zoom into the short-time behavior of the ACF. The solid lines are the nonviscous-membrane asymptote Eq. 4 in (D) and the viscous-membrane asymptote Eq. 5 in (E and F). t^* denotes the crossover time from relaxation dominated by bulk viscosity to membrane viscosity Eq. 3.

PS1 membranes are much more viscous. The long-time single exponential fits of the modes ACFs yield much higher dimensionless membrane viscosity, $\chi_s > 100$. Accordingly, their ACFs show clear $t^{3/4}$ power-law decay at short times. The fit of the short-time behavior with Eq. 5 yields viscosity $\chi_s = 150$ for the DPPC:Chol (7:3) membrane. However, the viscosity deduced from the long-time exponential decay of the ACF of each mode shows a trend to increase with the mode number, from $\chi_s = 180$ to 450. This more complex long-time dynamics may be a result from additional dissipation due to interpenetrating hydrophobic blocks of the two leaflets (43–45). The intermonolayer friction effect becomes more pronounced at shorter wavelengths thereby manifesting itself as a mode-dependent viscosity. This effect is absent in the current model, Eq. 1, which considers the membrane to be a structureless interface. Another possibility is diffusional softening in mixed bilayers (46–48) originating from a dynamic coupling between the lateral distribution of lipids with differing curvature preference and the membrane undulations.

The unique value for the viscosity obtained from the short-time fit with the ACF asymptote suggests it is the more reliable value.

Transverse Subdiffusion of a Membrane Segment and Dynamic Structure Factor of a Vesicle Membrane. While flickering spectroscopy measures the mean square displacement of the Fourier modes, scattering techniques such as neutron spin echo (49), dynamic light scattering (50), X-ray photon correlation spectroscopy (51) and some fluctuations experiments (52, 53) measure dynamic structure factor, $S(k, t)$, that is controlled by the single-point membrane MSD, $\langle (\Delta h(t))^2 \rangle$, $S(k, t) \sim \text{Exp}[-\frac{k^2}{2} \langle (\Delta h(t))^2 \rangle]$ (45, 54–56). Hence, it is instructive to

consider the effect of membrane viscosity on measurements made by these methods.

For planar membranes and nonviscous vesicles, the transverse (i.e. normal) membrane MSD, $\langle (\Delta h(t))^2 \rangle \equiv R^2 \langle (\Delta f(t))^2 \rangle$, follows the well-known prediction by Zilman and Granek (ZG) (54, 55),

$$\langle (\Delta h(t))^2 \rangle \simeq \frac{\Gamma[1/3]}{2\pi} \frac{k_B T}{\kappa^{1/3}} \left(\frac{t}{4\eta} \right)^{2/3}. \quad [10]$$

In contrast, for viscous vesicles, the ZG behavior is limited to earlier times, $t_0 \ll t \ll t^*$, and is absent altogether if $\chi_s \gtrsim R/d$. For longer times, $t^* \ll t \ll \eta_m R^2/\kappa$ and $\ell_{max} \gg 1$ (56), the MSD asymptotically exhibits subdiffusive behavior with exponent 1/2:

$$\langle (\Delta h(t))^2 \rangle \simeq \frac{R k_B T}{4\sqrt{\pi}} \left(\frac{t}{\kappa \eta_m} \right)^{1/2}. \quad [11]$$

It follows that the scattering from vesicles in this time range and large scattering wavenumbers, $kR \gg 1$, would still exhibit a stretched exponential DSF, $S(k, t) \approx \exp[-(\Gamma_k t)^\alpha]$, but with a modified stretching exponent α and relaxation rate Γ_k , changing from $\alpha = 2/3$ and $\Gamma_k \approx (k_B T)^{3/2} k^3 / \kappa^{1/2} \eta$ to $\alpha = 1/2$ and

$$\Gamma_k \approx (k_B T)^2 k^4 R^2 / \kappa \eta_m. \quad [12]$$

Indeed, the MSD (sometimes termed dynamic roughness) of DPPC:Chol (7:3) bilayer, shown in Fig. 4, follows the viscous behavior predicted by Eq. 11. Notably, there are no fitting parameters in this plot, as the value for the membrane viscosity is obtained from the analysis of the Fourier modes ACF shown in Fig. 3.

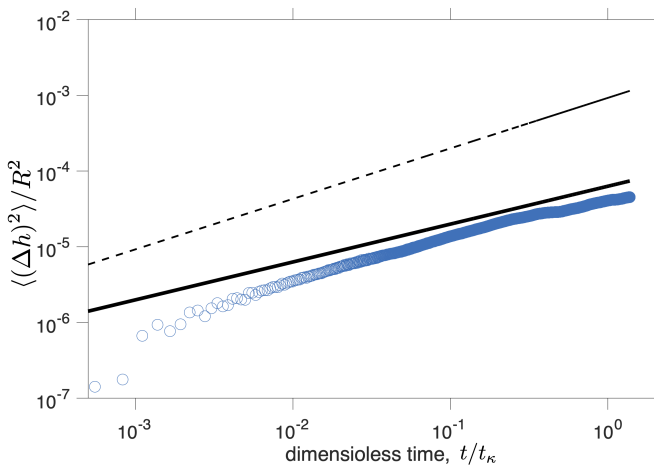


Fig. 4. Single-point membrane mean square displacement (dynamic roughness) of a DPPC:Chol (7:3) membrane. The solid line is the viscous asymptote Eq. 11 with $\chi_s = 150$, same as in Fig. 3. The dashed line is the nonviscous behavior Eq. 10.

This result may be of relevance to the discussion about the cholesterol stiffening of DOPC lipid bilayers reported from neutron spin echo (NSE) experiments but not found in flickering of giant vesicles (57, 58). Since the Saffman–Delbrück length even for typical low-viscosity lipid as DOPC is about a micron, the membrane dissipation affects the fluctuations of the submicron liposomes used in the NSE experiments. Currently, the NSE data are analyzed with the ZG model, which neglects membrane viscosity. Our results suggest that using the ZG model can misinterpret the effect of membrane viscosity as increased bending rigidity. A definitive answer, however, requires generalizing the theory to account for lipid density fluctuations (43–45, 59).

Polymer Membranes. The diblock-copolymer membranes display more complex dynamics. First, the apparent increase in viscosity with mode number is more pronounced and manifests itself in both the short-time and long-time dynamics. In Fig. 3 C and F, the long-time viscosity ranges from $\chi_s = 180$ to 1,100 and the short-time viscosity ranges between $\chi_s = 60$ and 280. Second, the viscosity obtained from the short-time asymptote tends to be lower than the one obtained from the single-exponential long-time ACF fit. Third, the ACF may exhibit multiple exponential decays. The PS1 membranes relax much more slowly compared to the DPPC:Chol (7:3) ones even though the lipid membrane has higher viscosity, because of much smaller bending rigidity (approximately by factor of 6). Accordingly, the long-time ACFs may be noisier. However, the mode dependence of the viscosity in the short-time ACFs suggests that additional dissipative mechanisms may be at play.

Fig. 5 compares the short-time ACFs of the lipid and polymer membranes. Rescaling the time by ν^4 , as suggested by Eqs. 8 and 9, collapses the data for the DPPC:Chol membrane—especially at short times, as implied by the weak ν dependence of the scaling function Eq. 9 at intermediate and long times—confirming that hydrodynamic dissipation in the membrane is solely responsible for the relaxation rate. The data collapse also suggests that the DPPC:Chol membranes behave as Newtonian fluids. The PS data, however, not only do not collapse but also exhibit crossover to relaxation with a lower exponent.

The more complex dynamics of the polymer membranes seen in the ACF behavior in Fig. 5B may result from several factors. In addition to intermonolayer friction (39, 44, 60–62), the membrane could be viscoelastic due to the slow polymer chain dynamics. Viscoelastic behavior of entangled and nonentangled polymer systems arises from different stress relaxation mechanisms. However, it is unclear which mechanism is responsible for the relaxation of the bilayer shear stress. The rheology of a sheared polymer brush along the normal ('z') axis has been studied extensively (see, e.g., ref. 63 and refs. therein), yet here we deal with the two-dimensional in-plane shear flow on which much less is known. Phenomenologically, if we assume a power-law complex modulus to describe the membrane viscoelasticity, $G_m^*(\omega) = G_0(i\omega\tau_m)^\alpha$, where τ_m is a relaxation time, it can be expected (following similar lines as in ref. 64) that the stretching exponent changes to $\zeta = \frac{3}{4}\alpha$. (In the case of Newtonian viscous fluid, $\alpha = 1$ and we recover $\zeta = 3/4$ and the membrane viscosity is $\eta_m = G_0\tau_m$.) While $\alpha = 1/2$ is predicted for the high-frequency Rouse chain dynamics, the Rouse time for a chain of N monomers scales as $\sim N^2$, and with $N \sim 40$ it is, therefore, likely orders of magnitude shorter than the experimental time scale, such that the power law $G_m^*(\omega)$ should be absent. Entangled chains take a much longer time to relax the stress they endure. Typically, the chains in the bilayer are expected to be weakly entangled similar to a polymer brush. If they nevertheless do entangle (65), the long (exponential in N) "arm retraction" time, similar to that appearing in the reptation of star polymers (66), might control the stress relaxation time, and this can give rise to a complicated viscoelastic behavior in the observation time scale. Finally, we pose the possibility that the membrane viscosity is wavelength, i.e. mode number ℓ , dependent, reflecting a more general system-size dependence property. The latter may explain the conflicting membrane viscosity values obtained from small system size simulations (67, 68) and measurements with giant vesicles (31, 39, 69). If so, the higher, long-time viscosity, seen in Fig. 3 B and D, reflects the longer wavelength viscosity, and suggests the expected value to be measured in electrodeformation and other large-scale flow experiments.

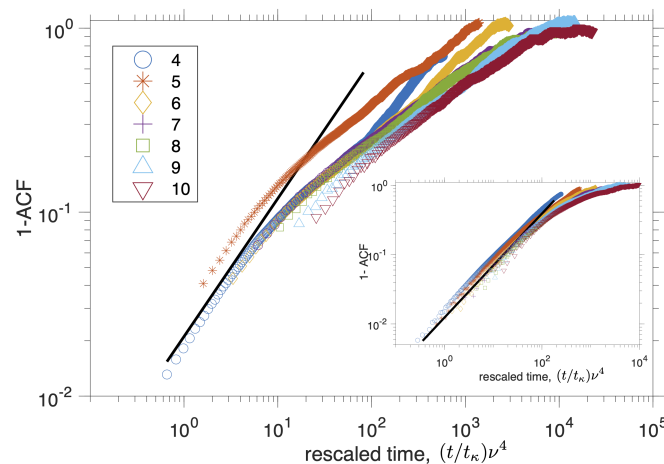


Fig. 5. Normalized mean square displacement for Fourier modes 4 to 10 of the fluctuating equatorial contour of a polymersome made of PS1 plotted as a function of the dimensionless time multiplied by the fourth power of the mode. *Inset:* Same plot but for DPPC:Chol vesicle showing collapse of the data. The solid line is the viscous asymptote Eq. 5 for tensionless membranes with $\chi_s = 150$. The time scale $t_k = \eta R^3/\kappa$.

Conclusions and Outlook

We show that membrane viscosity plays a significant role in the undulation dynamics of quasi-spherical vesicles if the Saffman–Delbrück length η_m/η is comparable to the vesicle radius R , that is $\chi_s \gtrsim 1$. This condition is met either when membrane viscosity is large, $\eta_m \gtrsim \eta R$, as in diblock-copolymer bilayers or lipid bilayers in the liquid-ordered phase such as DPPC:cholesterol, or when vesicle size is small, $R \lesssim \eta_m/\eta$, as in submicron liposomes.

The theory predicts that hydrodynamic dissipation within the membrane gives rise to a distinctive signature in the flickering spectrum of vesicles and liposomes. The time autocorrelation function of the Fourier modes, describing the contour fluctuations of the vesicle's equatorial cross-section, follows a stretched exponential decay with a universal stretching exponent of 3/4. This feature, combined with the variance of the fluctuations, allows for the independent measurement of membrane viscosity and bending rigidity from the flickering experiment—something usually impossible in scattering methods like NSE, where all physical parameters are inferred solely from the relaxation curves.

Applying the theory to flickering experiments of giant vesicles shows that DPPC:cholesterol membranes behave as a Newtonian fluid. In contrast, polymer membranes exhibit more complex rheological behavior, potentially due to viscoelasticity or interleaflet friction. To account for the latter, a theory analogous to the planar bilayer model (43) needs to be developed, incorporating membrane viscosity (59). This theory will also be relevant to NSE experiments (56), where χ_s becomes significant for the submicron liposomes used in this method, and lipid density relaxation due to bilayer slippage is important on the time scales of the curvature fluctuations (44, 45).

Our results highlight that the viscous properties of lipid bilayers significantly affect membrane bending dynamics, offering deeper insights into the dynamic aspects of curvature remodeling. The dynamic flickering experiment can serve as a noninvasive tool for the comprehensive analysis of membrane mechanics *in vitro*. This method can be applied to more complex membranes, such as asymmetric bilayers, hybrid lipid–polymer membranes, and charged membranes, to emulate conditions in both living and synthetic cells.

Materials and Methods

Vesicle Preparation. GUVs are formed from lipids such as pure DOPC, SOPC, mixtures of DPPC and Chol, and polymers such as poly(butadiene)-*b*-poly(ethylene oxide) diblock copolymers, PBd₁₃-*b*-PEO₁₁ (PS0) and PBd₂₂-*b*-PEO₁₄ (PS1). The lipids and diblock copolymer were purchased from Avanti Polar Lipids (Alabaster, AL) and Polymer Source Inc. (Montreal, Canada), respectively. The lipid vesicles were produced using the electroformation method (70). The stock solutions are diluted in chloroform to obtain a final concentration of 4 mM. Initially, 7 to 8 μ l of lipid solution is spread on the conductive side of two Indium tin oxide (Delta Technologies) glass slides with a 10 μ l gas-tight syringes (Hamilton, USA). The slides are placed inside vacuum to evaporate any leftover solvents for at least 3 h. Afterward, a 2 mm Teflon spacer is sandwiched between the two glass slides and the chamber is filled with 100 mM sucrose solution. The conductive sides of the slides are connected to AC signal generator Agilent 33220A (Agilent, Germany) at a voltage of 1.8 V_{pp} and 10 Hz. The connected chamber is placed inside an oven at 50 °C for 2 h. This procedure results in 10 to 50 μ m sized GUVs. The vesicle suspension is aspirated from the chamber and diluted in 110 mM glucose. Polymer vesicles were produced with the spontaneous swelling method. Initially, 50 μ l of 6 to 10 mg/ml (in chloroform)

polymer solution was dissolved in 200 to 300 μ l of chloroform in a 20 ml vial. Polymer films were formed from evaporation by blowing with a nitrogen stream while swirling the solution inside. Afterward, the vials were dried under vacuum for 2 to 4 h. The polymer films were hydrated in the suspending solutions (100 mM sucrose solution) and placed at 60 °C in an oven for 18 to 24 h.

Optical Microscopy and Imaging. The shape fluctuations of a GUV are visualized in phase contrast mode with Axio Observer A1 microscope (Zeiss, Germany). The microscope objectives used are Plan-Apochromat 100×/1.4 Oil Ph3 M27, with Immersol 518 Foil, and 63×(0.75 NA) Ph2(air) (Zeiss, Germany). Focal depth (FD) or full-width half maximum of phase contrast imaging for our setting is determined using the standard formula $FD = \frac{\lambda}{NA^2}$. For a wavelength of transmission light $\lambda = 550$ nm, the calculated FD for the 100× observations is 281 nm.

Electrodeformation Method Measure Membrane Viscosity. We implement the transient electrodeformation of GUVs to measure membrane viscosity (31). To summarize, the harvested GUVs are diluted in 510 mM Glucose solution without any salt in an Eppendorf electrofusion chamber (Eppendorf, Germany) containing two Pt electrodes spaced 500 μ m apart. The method involves measuring the initial deformation rate of a vesicle as AC electric field is applied at a particular frequency. High-speed imaging of the increase of the vesicle aspect ratio, δ , is done at 1 to 2 kfps. The linear slope of the aspect ratio as a function of time depends on membrane viscosity as $\delta = 1 + t \left(\frac{3p(\omega)\epsilon E_0^2}{\eta(55+16\chi_s)} \right)$, where

$\chi_s = \eta_m/\eta R$ is the dimensionless membrane viscosity η_m , η is the viscosity the solution inside and outside the vesicle, E_0 is the electric field amplitude and $p(\omega)$ is the electric pressure detailed in Faizi et al. (31). The apparent viscosities are measured at different frequencies in the range 0.1 to 1 kHz. The zero-frequency viscosity is obtained by extrapolating a linear fit of the viscosity vs. frequency data. Electric field of 8 kV/m produces a good range of data in the linear initial slope.

Flickering Experiment. The vesicle equatorial contour is fitted by a Fourier series $r_s = \sum_{v=0}^{v_{max}} \alpha_v \cos(v\theta) + \beta_v \sin(v\theta)$. The second mode in the series is used to determine the major (a) and minor axis (b) of the deformed vesicles to evaluate the aspect ratio $\delta = \frac{a}{b} = (1 + \alpha_2)/(1 - \alpha_2)$. To ensure good statistics for the ACF, images of the fluctuating contour are acquired at 50 to 500 fps for 5 to 10 min, for a total of 0.1 to 0.5 million images. Only vesicles with low tension value in the range 10^{-8} to 10^{-10} N/m are chosen. This results in shape fluctuations that are dominated by bending rigidity. Details about the experiment can be found in refs. 35, 36, 71 and *SI Appendix*.

Data, Materials, and Software Availability. Experimental data can be accessed at Northwestern's ARCH Research and Data Repository (72).

ACKNOWLEDGMENTS. P.M.V. and H.A.F. acknowledge financial support by NIH award 1R01GM140461. This research was also supported in part by the NSF under Grant NSF PHY-1748958 and the National Institute for Mathematics and Theory in Biology (Simons Foundations award MP-TMPS-00005320 and NSF award DMS-2235451). R.G. is grateful to Northwestern University's Department of Engineering Sciences and Applied Mathematics for its hospitality during the period when this research was completed.

Author affiliations: ^aDepartment of Mechanical Engineering, Northwestern University, Evanston, IL 60208; ^bAvram and Stella Goldstein-Goren Department of Biotechnology Engineering, and Ilse Katz Institute for Nanoscale Science and Technology, Ben-Gurion University of The Negev, Beer Sheva 84105, Israel; ^cDepartment of Engineering Sciences and Applied Mathematics, Northwestern University, Evanston, IL 60208; and ^dNational Institute for Theory and Mathematics in Biology, Northwestern University and The University of Chicago, Chicago, IL 60611

1. R. Lipowsky, The conformation of membranes. *Nature* **349**, 475–481 (1991).
2. B. C. Buddingh', J. C. M. van Hest, Artificial cells: Synthetic compartments with life-like functionality and adaptivity. *Account. Chem. Res.* **50**, 769–777 (2017).
3. E. Rideau, R. Dimova, P. Schwille, F. R. Wurm, K. Landfester, Liposomes and polymersomes: A comparative review towards cell mimicking. *Chem. Soc. Rev.* **47**, 8572–8610 (2018).
4. P. Bassereau *et al.*, The 2018 biomembrane curvature and remodeling roadmap. *J. Phys. D Appl. Phys.* **51**, 343001 (2018).
5. J. S. Bonifacino, B. S. Glick, The mechanisms of vesicle budding and fusion. *Cell* **116**, 153–166 (2004).
6. H. T. McMahon, J. L. Gallop, Membrane curvature and mechanisms of dynamic cell membrane remodelling. *Nature* **438**, 590–596 (2005).
7. L. V. Chernomordik, M. M. Kozlov, Mechanics of membrane fusion. *Nat. Struct. Mol. Biol.* **15**, 675–683 (2008).
8. M. M. Kozlov, J. W. Taraska, Generation of nanoscopic membrane curvature for membrane trafficking. *Nat. Rev. Mol. Cell Biol.* **24**, 63–78 (2023).
9. R. Lipowsky, Remodeling of membrane shape and topology by curvature elasticity and membrane tension. *Adv. Biol.* **6**, 2101020 (2022).
10. A. Zidovska, E. Sackmann, Brownian motion of nucleated cell envelopes impedes adhesion. *Phys. Rev. Lett.* **96**, 048103 (2006).
11. S. F. Fenzl *et al.*, Membrane fluctuations mediate lateral interaction between cadherin bonds. *Nat. Phys.* **13**, 906–913 (2017).
12. F.-Y. Chu, S. C. Haley, A. Zidovska, On the origin of shape fluctuations of the cell nucleus. *Proc. Natl. Acad. Sci. U.S.A.* **114**, 10338–10343 (2017).
13. J. A. Jackson *et al.*, Scaling behaviour and control of nuclear wrinkling. *Nat. Phys.* **19**, 1927+ (2023).
14. U. Seifert, Configurations of fluid membranes and vesicles. *Adv. phys.* **46**, 13–137 (1997).
15. C. Monzel, K. Sengupta, Measuring shape fluctuations in biological membranes. *J. Phys. D Appl. Phys.* **49**, 243002 (2016).
16. H. Turlier, T. Betz, Unveiling the active nature of living-membrane fluctuations and mechanics. *Annu. Rev. Condens. Matter Phys.* **10**, 213–232 (2019).
17. S. Gupta, R. Ashkar, The dynamic face of lipid membranes. *Soft Matter* **17**, 6910–6928 (2021).
18. F. Brochard, J. F. Lennon, Frequency spectrum of the flicker phenomenon in erythrocytes. *J. Phys. Fr.* **36**, 1035–1047 (1975).
19. P. Olla, The behavior of closed inextensible membranes in linear and quadratic shear flows. *Phys. A* **278**, 87–106 (2000).
20. S. B. Rochal, V. L. Lorman, G. Mennessier, Viscoelastic dynamics of spherical composite vesicles. *Phys. Rev. E* **71**, 021905 (2005).
21. M. L. Henle, A. J. Levine, Hydrodynamics in curved membranes: The effect of geometry on particulate mobility. *Phys. Rev. E* **81**, 011905 (2010).
22. F. G. Woodhouse, R. E. Goldstein, Shear-driven circulation patterns in lipid membrane vesicles. *J. Fluid Mech.* **705**, 165–175 (2012).
23. M. Rahimi, A. DeSimone, M. Arroyo, Curved fluid membranes behave laterally as effective viscoelastic media. *Soft Matter* **9**, 11033–11045 (2013).
24. M. Rahimi, "Shape dynamics and lipid hydrodynamics of bilayer membranes: Modeling, simulation and experiments," PhD thesis, Universitat Politècnica de Catalunya (2013).
25. J. K. Sigurdsson, P. J. Atzberger, Hydrodynamic coupling of particle inclusions embedded in curved lipid bilayer membranes. *Soft Matter* **12**, 6685–6707 (2016).
26. P. M. Vlahovska, "Dynamics of membrane bound particles: capsules and vesicles" in *Low-Reynolds-Number Flows: Fluid-Structure Interactions*, C. Duprat and H.A. Stone Eds. (Royal Society of Chemistry Series RSC Soft Matter, 2016).
27. A. Sahu, A. Glisman, J. Tchoufag, K. K. Mandapadu, Geometry and dynamics of lipid membranes: The screen-lover number. *Phys. Rev. E* **101**, 052401 (2020).
28. P. M. Vlahovska, Electrohydrodynamics of drops and vesicles. *Annu. Rev. Fluid Mech.* **51**, 305–330 (2019).
29. S. T. Milner, S. A. Safran, Dynamical fluctuations of droplet microemulsions and vesicles. *Phys. Rev. A* **36**, 4371–4379 (1987).
30. S. Komura, K. Seki, Dynamical fluctuations of spherically closed fluid membranes. *Phys. A* **192**, 27–46 (1993).
31. H. A. Faizi, R. Dimova, P. M. Vlahovska, A vesicle micro rheometer for high-throughput viscosity measurements of lipid and polymer membranes. *Biophys. J.* **121**, 910–918 (2022).
32. R. Dimova, C. Dietrich, A. Hadjilijsky, K. Danov, B. Pouliquen, Falling ball viscosimetry of giant vesicle membranes: Finite-size effects. *Euro. Phys. J. B* **12**, 589–598 (1999).
33. G. J. Amador, D. V. Dijk, R. Kieffer, M.-E. Aubin-Tam, D. Tam, Hydrodynamic shear dissipation and transmission in lipid bilayers. *Proc. Natl. Acad. Sci. U.S.A.* **118**, e2100156118 (2021).
34. R. Dimova, U. Seifert, B. Pouliquen, S. Förster, H.-G. Dobereiner, Hyperviscous diblock copolymer vesicles. *Eur. Phys. J. E* **7**, 241–250 (2002a).
35. R. S. Gracia, N. Bezlyepkina, R. L. Knorr, R. Lipowsky, R. Dimova, Effect of cholesterol on the rigidity of saturated and unsaturated membranes: Fluctuation and electrodeformation analysis of giant vesicles. *Soft Matter* **6**, 1472–1482 (2010).
36. H. A. Faizi, C. J. Reeves, V. N. Georgiev, P. M. Vlahovska, R. Dimova, Fluctuation spectroscopy of giant unilamellar vesicles using confocal and phase contrast microscopy. *Soft Matter* **16**, 8996–9001 (2020).
37. J. Peceaux, H.-G. Dobereiner, J. Prost, J.-F. Joanny, P. Bassereau, Refined contour analysis of giant unilamellar vesicles. *Eur. Phys. J. E* **13**, 277–290 (2004).
38. Y. Wang, P. Gkeka, J. E. Fuchs, K. R. Liedl, Z. Cournia, DPPC-cholesterol phase diagram using coarse-grained molecular dynamics simulations. *Biochim. Biophys. Acta* **1858**, 2846–2857 (2016).
39. R. Dimova, U. Seifert, B. Pouliquen, S. Förster, H.-G. Dobereiner, Hyperviscous diblock copolymer vesicles. *Eur. Phys. J. D* **7**, 241–250 (2002b).
40. E. G. Kelley, P. D. Butler, R. Ashkar, R. Bradbury, M. Nagao, Scaling relationships for the elastic moduli and viscosity of mixed lipid membranes. *Proc. Natl. Acad. Sci. U.S.A.* **117**, 23365–23373 (2020).
41. E. Farge, A. C. Maggs, Dynamic scattering from semiflexible polymers. *Macromolecules* **26**, 5041–5044 (1993).
42. R. Granek, From semi-flexible polymers to membranes: Anomalous diffusion and reptation. *J. Phys. B* **7**, 1761–1788 (1997).
43. U. Seifert, S. A. Langer, Viscous modes of fluid bilayer membranes. *Europhys. Lett.* **23**, 71–76 (1993).
44. M. C. Watson, F. L. H. Brown, Interpreting membrane scattering experiments at the mesoscale: The contribution of dissipation within the bilayer. *J. Chem. Phys.* **98**, L9–L11 (2010).
45. M. C. Watson, Y. Peng, Y. Zheng, F. L. H. Brown, The intermediate scattering function for lipid bilayer membranes: From nanometers to microns. *J. Chem. Phys.* **135**, 194701 (2011).
46. H. J. Lessen, K. C. Sapp, A. H. Beaven, R. Ashkar, A. J. Sodt, Molecular mechanisms of spontaneous curvature and softening in complex lipid bilayer mixtures. *Biophys. J.* **121**, 3188–3199 (2022).
47. K. Sapp, M. Aleksanyan, K. Kerr, R. Dimova, A. Sodt, Kinetic relaxation of giant vesicles validates diffusional softening in a binary lipid mixture. *Phys. Rev. E* **107**, 054403 (2023).
48. A. Hosseini, A. H. Beaven, K. Sapp, A. J. Sodt, Softening in two-component lipid mixtures by spontaneous curvature variance. *J. Phys. Chem. B* **128**, 6317–6326 (2024).
49. M. Nagao, E. G. Kelley, R. Ashkar, R. Bradbury, P. D. Butler, Probing elastic and viscous properties of phospholipid bilayers using neutron spin echo spectroscopy. *J. Phys. Chem. Lett.* **8**, 4679–4684 (2017).
50. E. Freyssingeas, D. Roux, Quasi-elastic light scattering study of highly swollen lamellar and "sponge" phases. *J. Phys.* **7**, 913–929 (1997).
51. P. Falus, M. A. Borthwick, S. G. J. Moohrie, Fluctuation dynamics of block copolymer vesicles. *Phys. Rev. Lett.* **94**, 016105 (2005).
52. T. Betz, C. Sykes, Time resolved membrane fluctuation spectroscopy. *Soft Matter* **8**, 5317–5326 (2012).
53. E. Helfer *et al.*, Microrheology of biopolymer-membrane complexes. *Phys. Rev. Lett.* **85**, 457–460 (2000).
54. A. G. Zilman, R. Granek, Undulations and dynamic structure factor of membranes. *Phys. Rev. Lett.* **77**, 4788–4791 (1996).
55. A. G. Zilman, R. Granek, Membrane dynamics and structure factor. *Chem. Phys.* **284**, 195–204 (2002).
56. R. Granek *et al.*, Dynamic structure factor of undulating vesicles: Finite-size and spherical geometry effects with application to neutron spin echo experiments. *Eur. Phys. J. E* **47**, 12 (2024).
57. S. Chakraborty *et al.*, How cholesterol stiffens unsaturated lipid membranes. *Proc. Natl. Acad. Sci. U.S.A.* **117**, 21896–21905 (2020).
58. J. F. Nagle *et al.*, A needless but interesting controversy. *Proc. Natl. Acad. Sci. U.S.A.* **118**, e2025011118 (2021).
59. L. Miao, M. A. Lomholt, J. Kleis, Dynamics of shape fluctuations of quasi-spherical vesicles revisited. *Eur. Phys. J. E* **9**, 143–160 (2002).
60. R. Rodríguez-García *et al.*, Bimodal spectrum for the curvature fluctuations of bilayer vesicles: Pure bending plus hybrid curvature-dilation modes. *Phys. Rev. Lett.* **102**, 128101 (2009).
61. M. Mell *et al.*, Fluctuation dynamics of bilayer vesicles with intermonolayer sliding: Experiment and theory. *Chem. Phys. Lipids* **185**, 61–77 (2015).
62. A. A. Anthony, O. Sahin, M. K. Yapici, D. Rogers, A. R. Honerkamp-Smith, Systematic measurements of interleaflet friction in supported bilayers. *Biophys. J.* **121**, 2981–2993 (2022).
63. P. S. Doyle, E. S. G. Shaqfeh, A. P. Gast, Rheology of polymer brushes: A brownian dynamics study. *Macromolecules* **31**, 5474–5486 (1998).
64. R. Granek, Membrane surrounded by viscoelastic continuous media: Anomalous diffusion and linear response to force. *Soft Matter* **7**, 5281–5289 (2011).
65. R. S. Hoy, G. S. Grest, Entanglements of an end-grafted polymer brush in a polymeric matrix. *Macromolecules* **40**, 8389–8395 (2007).
66. M. Doi, S. F. Edwards, *The Theory of Polymer Dynamics* (Oxford University Press, 1988).
67. A. Zgorski, R. W. Pastor, E. Lyman, Surface shear viscosity and interleaflet friction from nonequilibrium simulations of lipid bilayers. *J. Chem. Theory Comput.* **15**, 6471–6481 (2019).
68. J. E. Fitzgerald, R. M. Venable, R. W. Pastor, E. R. Lyman, Surface viscosities of lipid bilayers determined from equilibrium molecular dynamics simulations. *Biophys. J.* **122**, 1094–1104 (2023).
69. A. R. Honerkamp-Smith, F. G. Woodhouse, V. Kantsler, R. E. Goldstein, Membrane viscosity determined from shear-driven flow in giant vesicles. *Phys. Rev. Lett.* **111**, 038103 (2013).
70. M. I. Angelova, D. S. Dimitrov, Liposome electroformation. *Faraday Discuss. Chem. Soc.* **81**, 303–311 (1986).
71. H. A. Faizi, S. L. Frey, J. Steinkuehler, R. Dimova, P. M. Vlahovska, Bending rigidity of charged lipid bilayer membranes. *Soft Matter* **15**, 6006–6013 (2019).
72. P. M. Vlahovska, Data for "Curvature fluctuations of fluid vesicles reveal hydrodynamic dissipation within the bilayer". Northwestern Arch Research and Data Repository. <https://doi.org/10.21985/n2-a0g5-ch76>. Deposited 26 September 2024.